Supplementary Material

High-Efficiency MEMS Synthetic Jet Cooler for Mobile Thermal Management

These materials aim to enhance the clarity and reproducibility of our method.

1. Supplementary Equations S1 to S10 (Detailed process of deriving Eq. (2)):

Distance from the center of the Si layer to the centerline of the composite plane neutral layer:

$$h_s = \left|\frac{H_1}{2} - h\right| \tag{S1}$$

The coordinate along the *z*-axis, which is the central axis of the composite neutral layer, is [27]:

$$h = \frac{\sum_i E_i y_i H_i}{\sum_i E_i H_i} \tag{S2}$$

substituting yields:

$$h_e = \frac{E_1 H_1 (H_1 + H_2)}{2(E_1 H_1 + E_2 H_2)} \tag{S3}$$

E_i and y_i represent the Young's modulus and the position of the plane within the i_{th} layer, respectively. When a drive voltage *U* is applied between the top electrode and the bottom electrode, the composite bending moment *M(x)* is given by:

$$M(x) = -e_{31} U W h_e \tag{S4}$$

The upper and lower films have the same radius of curvature and satisfy the following conditions:

$$R_0 = \frac{d^2 w}{dx^2} = -\frac{M(x)}{EI(x)} \tag{S5}$$

Here, *EI(x)* and *I(x)* represent the bending stiffness of the multilayer plate and the moment of inertia of each layer, respectively:

$$EI(x) = \sum_i E_i I_i(x) \tag{S6}$$

$$I_i(x) = \frac{{t_i}^3 + 12 t_i (y_i - h)^2}{12} W \tag{S7}$$

substituting yields [28]:

$$\frac{d^2 w}{dx^2} = -\frac{12 M(x)}{WK} \tag{S8}$$

$$K = \sum_i E_i\left({t_i}^3 + 12 t_i (y_i - h)^2\right) \tag{S9}$$

The boundary conditions for a simply supported cantilever beam are as follows when *x*

= 0 [25]:

$$\begin{cases} \dfrac{dw}{dx} = 0 \\ w = 0 \end{cases} \tag{S10}$$

substituting the integral yields the expression for the static deflection of a composite rectangular cantilever beam under voltage *U*:

$$w_0(x) = \left| \frac{6e_{31}h_eU}{K}x^2 \right| \tag{2}$$

2.Supplementary Figures S1 to S2:

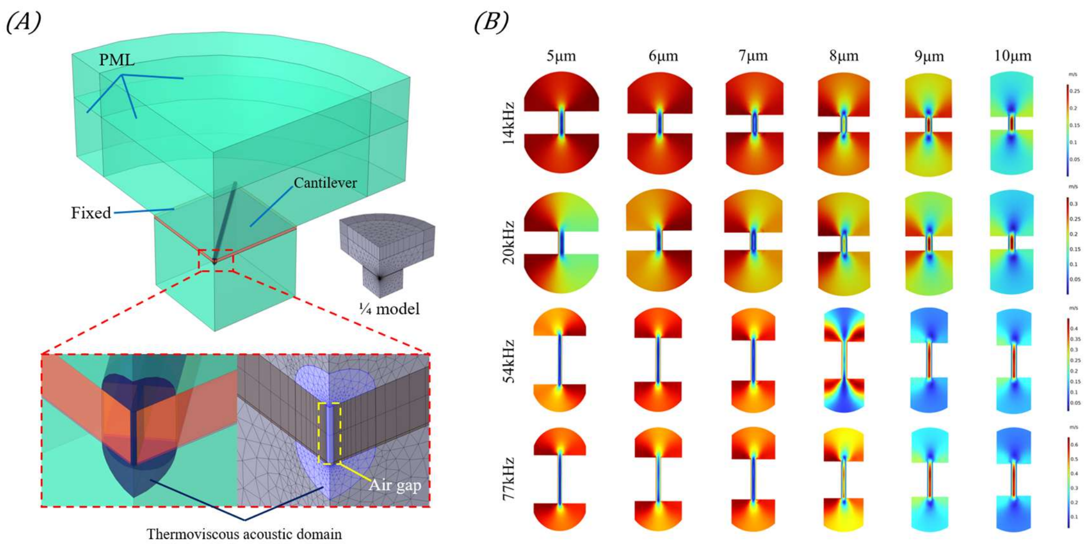

sFig. 1 Thermoviscous acoustic simulation results. (A) Finite element simulation model and corresponding mesh configuration. **(B)** Effects of different frequencies and air gap widths on the degree of gas leakage.

To investigate the design of the acoustic barrier width, a numerical model of the piezoelectric MEMS ejector was established in this study based on the piezoelectric MEMS loudspeaker benchmark available in the COMSOL Multiphysics library, with the number of cantilever beams set to n = 4, as schematically illustrated in Fig. S1A. To alleviate the computational cost and memory demand inherent in three-dimensional finite element simulations, a quarter-symmetry simplification was adopted. A fixed constraint condition was applied to the bottom surface of the cantilever beams, and multiple perfectly matched layers (PML) were placed at the outer boundaries of the computational domain to absorb outgoing acoustic pressure. The air gap and its adjacent cylindrical region were defined as thermoviscous acoustic domains. Transient simulations were then performed based on the established model to compute the acoustic pressure distribution on both sides of the cantilever beams. For the sake of clarity, only two cantilever beams and one air gap are shown in the figure, highlighting the thermoviscous acoustic behavior in the vicinity of the air gap.

Four actuator configurations with distinct resonant frequencies were generated by combining cantilever widths of 2.5 mm and 3 mm with device layer thicknesses of 15 μm and 50 μm. By varying the gap width, the resulting fluid velocity distributions near the gap were calculated, with the outcomes presented in Fig. S1B. The simulation results concerning the influence of gap width on thermoviscous acoustics and pressure acoustics indicate the following. At all four frequencies, when the gap width is less than 8 μm, the fluid velocity within the gap channel remains substantially lower than that on both external sides, suggesting that the diaphragm, under common-mode motion, can be treated as a sealed, leak-free single-layer membrane. When the gap width equals 8 μm, the fluid velocity inside the channel increases noticeably, indicating the occurrence of minor leakage, and the diaphragm may thus be regarded as a single-layer membrane with slight leakage. For gap widths exceeding 8 μm, air leakage becomes increasingly pronounced as the gap width widens, and the associated leakage loss exhibits frequency dependence. Specifically, structures operating at higher frequencies demonstrate superior sealing performance relative to their lower-frequency counterparts. Finally, taking into account the etching tolerances that may arise during practical fabrication, a gap width of 6 μm was ultimately selected as the design value.

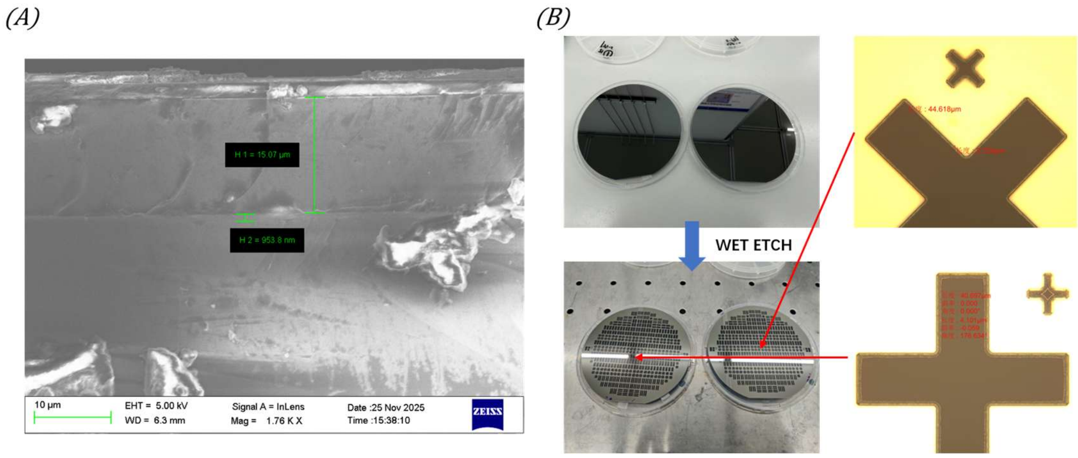

sFig. 2 Materials and methods used in device fabrication. (A) Cross-sectional SEM image of the SOI wafer used. **(B)** Result of the wet etching process adopted in this work.

During device fabrication, the thicknesses of the device layer (15μm) and the buried oxide layer (1μm) of the employed SOI wafer were measured, as shown in Fig. S2A. In the patterning process of the PZT layer (Fig. S2B), an optimized wet etching method was adopted, which resulted in a negligible lateral etching distance and yielded well-defined PZT patterns with favorable morphology. This is crucial for ensuring satisfactory piezoelectric performance of the actuator.